Geophysical Research Letters

RESEARCH LETTER
10.1002/2018GL077298

Evidence for Neutrals-Foreshock Electrons Impact at Mars

C. X. Mazelle[1], K. Meziane[1,2], D. L. Mitchell[3], P. Garnier[1], J. R. Espley[4], A. M. Hamza[2], J. Halekas[5], and B. M. Jakosky[6]

[1]IRAP, Université de Toulouse, CNRS, UPS, CNES, Toulouse, France, [2]Physics Department, University of New Brunswick, Fredericton, New Brunswick, Canada, [3]Space Sciences Laboratory, University of California, Berkeley, CA, USA, [4]NASA Goddard Space Center, Greenbelt, MD, USA, [5]Department of Physics and Astronomy, University of Iowa, Iowa City, IA, USA, [6]Laboratory for Atmospheric and Space Physics, University of Colorado Boulder, Boulder, CO, USA

Key Points:
- Foreshock electrons flux declines with the distance from the shock of Mars
- Martian foreshock electron flux ratios are consistent with the electron-neutral hydrogen impact cross section
- Foreshock electrons play an important role in the production of pickup ions in Mars distant exosphere

Correspondence to:
C. X. Mazelle,
cmazelle@irap.omp.eu

Citation:
Mazelle, C. X., Meziane, K., Mitchell, D. L., Garnier, P., Espley, J. R., Hamza, A. M., et al. (2018). Evidence for neutrals-foreshock electrons impact at Mars. *Geophysical Research Letters*, *45*. https://doi.org/10.1002/2018GL077298

Received 26 JAN 2018
Accepted 20 MAR 2018
Accepted article online 26 MAR 2018

Abstract Backstreaming electrons emanating from the bow shock of Mars reported from the Mars Atmosphere and Volatile EvolutioN/Solar Wind Electron Analyzer observations show a flux fall off with the distance from the shock. This feature is not observed at the terrestrial foreshock. The flux decay is observed only for electron energy $E \geq 29$ eV. A reported recent study indicates that Mars foreshock electrons are produced at the shock in a mirror reflection of a portion of the solar wind electrons. In this context, and given that the electrons are sufficiently energetic to not be affected by the interplanetary magnetic field fluctuations, the observed flux decrease appears problematic. We investigate the possibility that the flux fall off with distance results from the impact of backstreaming electrons with Mars exospheric neutral hydrogen. We demonstrate that the flux fall off is consistent with the electron-atomic hydrogen impact cross section for a large range of energy. A better agreement is obtained for energy where the impact cross section is the highest. One important consequence is that foreshock electrons can play an important role in the production of pickup ions at Mars far exosphere.

Plain Language Summary Energetic electrons emanating from the bow shock surrounding Mars by reflection of a small portion of the incident solar wind display an enigmatic decrease with the distance along the interplanetary magnetic field. We show for the first time from measurements by the MAVEN SWEA instrument that this is a consequence of the impact of those electrons on the neutrals atoms of the upper atmosphere of the planet. The signature of this process on the energetic electrons can be used as new diagnostic of the far upper atmosphere to better investigate the atmospheric escape.

1. Introduction

A recent study based on Mars Atmosphere and Volatile EvolutioN (MAVEN) data revealed that the entire bow shock surface of Mars forms a source for backstreaming electrons with energies reaching up to ~2 keV (Meziane et al., 2017). The backstreaming electrons appear as ring beams in velocity space strongly indicating that the magnetic mirroring of a portion of solar wind electrons taking place at the shock is a plausible mechanism for their production. In addition, the study shows that the electron flux falls off with distance from the shock and decreases with increasing shock-θ_{Bn}, the angle that the shock normal makes with the upstream ambient magnetic field. The last aspect appears somewhat problematic since in the mirror reflection mechanism, maximum efficiency occurs for a nearly perpendicular shock (Leroy & Mangeney, 1984; Vandas, 2001). Also and in several respects, the foreshock electrons flux fall off with distance seems quite remarkable. At first glance, electron beams from tens to several hundreds of eV emanating from shock are expected to propagate a considerable distance beyond MAVEN's orbit before the effects of scattering by magnetic field fluctuations become measurable. There is no evidence for plasma waves that could efficiently scatter the electron beams. In this report, we provide evidence that the foreshock electron flux decrease with distance is due to collisions with the extended exospheric neutral hydrogen of Mars.

Because of the lack of a global magnetic field at Mars, the solar wind can directly interact with the upper atmosphere, inducing ion escape via ionization, sputtering. and pickup processes (Jakosky et al., 2015; Rahmati, 2016). Mars atmospheric loss is driven by several mechanisms (Brain & Jakosky, 1998; Lundin et al., 1989). Ion pickup process is the focus of our present study. In this process, neutral atoms are ionized and "picked up" by the solar wind embedded magnetic field. Several sources of ionization are possible. In the exosphere

upstream of the bow shock, photoionization and charge exchange are the dominant mechanisms, with ionization through electron impact providing a minor contribution (Rahmati, 2016). In this mechanism, free electrons collide with neutral atoms, and if the energy of the former is higher than the ionization threshold of the latter, an ion can be produced. The collision cross section indicates the relevance of the impact process, and it is expected that the solar wind electron impact neutral ionization remains weak upstream of the bow shock. With a temperature of ~10 eV, most of the solar wind electron flux remains below the level for which the cross section for electron impact ionization for hydrogen peaks (~50 eV) (Baertschy et al., 2001). Using Solar Wind Electron Analyzer (SWEA) data, Rahmati (2016) estimated that the neutral hydrogen electron impact process provides the smallest ionization frequency in the solar wind.

At first glance, the exospheric neutral atoms impact with foreshock electrons may appear quite minor as the foreshock electron density is significantly much smaller comparatively to the solar wind electron density. Nevertheless, the flux of foreshock electrons with an energy above the ionization threshold exceeds that of the solar wind and is significantly enhanced up to a few hundreds of eV in the energy range where electron impact ionization is important. In the present letter, quantitative arguments are developed in support of foreshock electrons impact with exospheric hydrogen. In the next section, the observations are presented and the comparison with the impact hypothesis is developed in section 4.

2. MAVEN Data

The MAVEN mission's main objective consists of understanding the escape of volatile gas at Mars through the interaction of the solar wind with the upper atmosphere (Jakosky et al., 2015). In this study, we focus on data from the SWEA and the magnetometer (MAG). SWEA consists of a symmetrical hemispheric-shaped detector able to measure the energy and angular distributions of 3–4,600 eV electrons throughout the Mars environment. The instrument field of view spans 80% of all sky and a distribution function is obtained in every 32 s while the integrated flux is collected every 4 s near the shock, typically, the cadence depending on altitude and Mars-Earth distance (Mitchell et al., 2016). The MAG sensors measure the vector magnetic field with a precision of ~0.35 nT and a sampling rate of 32 Hz (Connerney et al., 2015), sufficiently enough to study the dominant ion scale plasma processes occurring at the bow shock of Mars.

3. Observations

The first event examined in the present study has been extensively discussed in a previous work, which shows typical particle and field measurements upstream of the bow shock of Mars (Meziane et al., 2017). A time series of electron flux for four selected energy ranges are shown on the first panel of Figure 1 as recorded by MAVEN/SWEA on 2 January 2015 between 1635 UT and 1830 UT. An outbound shock transition crossing occurs approximately between 1639 UT and 1642 UT as indicated by the vertical black dashed line. The local geometry is clearly quasi-parallel as confirmed by the model (Vignes et al., 2000) with low values of the local angle between the shock normal and the upstream magnetic field direction (see Figure 3 of Meziane et al., 2017). This implies a large thickness of the shock transition and makes its precise location difficult to be defined. However, the left black dashed line marks the exit from the magnetosheath revealed by a general increase of the electron fluxes for all energies including the lowest range with a large increase of their fluctuation amplitude as well as much larger magnetic fluctuations and magnitude (off-scale on second and third panels). The right black dashed line coincides with the location of the shock given by the model. After that, the spacecraft is continuously within the foreshock region until 1802 UT, just before apoapsis at 1820 UT. Between 1802 UT and 1830 UT MAVEN is in the unperturbed solar wind. The successive panels of Figure 1 show the Mars Solar Orbit (MSO) components and the magnitude of the interplanetary magnetic field (IMF), the foreshock depth *DIF* (the distance parallel to the *X* direction of the spacecraft position from the IMF tangent line to the shock), the distance *DIST* along the ambient magnetic field between MAVEN and the shock, and the planetocentric distance *R* of MAVEN. Vignes et al. (2000) is used for the determination of *DIST* and *DIF*. A negative numerical value of the latter parameter indicates that MAVEN is not magnetically connected to the shock. It is remarkable that Vignes et al. (2000) bow shock model satisfactorily reproduces the MAVEN shock crossing and the magnetic disconnection that occurs simultaneously with the discontinuation of foreshock electrons flux at 1802 UT. Figure 1 shows a moderate but noticeable flux decrease with *DIST* and *R* for electrons $E > 30$ eV (see also Figure 3 of Meziane et al. (2017)). The decrease in >30-eV electron flux can be seen more clearly when plotted versus *DIST* (Figure 2). The fluxes in two energy ranges (46–59 and 74–94 eV) fall off steeply within ~1 R_M of the shock as the electrons move sunward along the IMF direction.

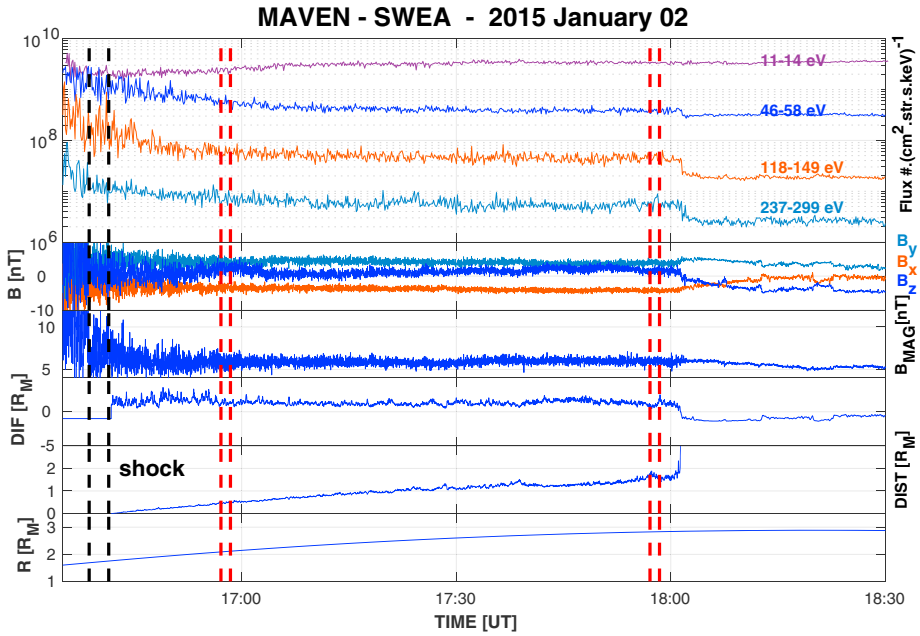

Figure 1. The first to sixth panels respectively show the electron flux for four selected energy ranges, the MSO-IMF components, the magnetic field magnitude, the distance *DIST* along the ambient IMF of MAVEN to the shock, the foreshock depth *DIF*, and the planetocentric distance *R* of MAVEN.

4. Impact With Neutrals Hypothesis

Plausible physical mechanisms can be advanced to account for the electron flux decrease with distance upstream of the shock. One possibility is that the electron flux decrease results from the shock source due to the geometry monotonic change. Clearly in the 2 January 2015 event, the electron flux decay is accompanied by an increase of the shock-θ_{Bn} from 20° to ~90° (Meziane et al., 2017). However, this apparent association is not always observed. In addition, if the foreshock electrons result from quasi-adiabatic reflection off the shock, it is expected that the flux level at nearly perpendicular shock (θ_{Bn} ~90°) exceeds the one at quasi-parallel shock. Another possibility suggests that the electron beams emanating from the shock are efficiently scattered by plasma waves and IMF fluctuations in the foreshock. This possibility is problematic since wave scattering of electrons is expected to be negligible on MAVEN orbital distance scale given the high speed of the backstreaming electrons. In this section, we investigate whether the observed electron flux decrease with distance from the shock results from the impact with exospheric atomic hydrogen. For this purpose, we use a simple heuristic model involving particle collisions.

We consider a monoenergetic beam of electrons with energy E emanating from the shock and colliding with a neutral exospheric atomic hydrogen. At a distance x from the shock, the variation of electron flux $\Gamma_E(x)$ as the electrons propagate through the exosphere can be governed by the following expression (Chen, 1984):

$$\frac{d\Gamma_E(x)}{dx} = -n_H(r(x))\sigma(E)\Gamma_E(x) \tag{1}$$

where $n_H(r(x))$ is the atomic hydrogen density profile and $\sigma(E)$ the collision electron cross section. It is implicitly assumed that the exospheric hydrogen is at rest and the electrons propagate along the magnetic field direction x. We, however, emphasize that the hydrogen density profile is given in terms of the planetocentric distance r. The relation between r and x is obtained from the direction of the IMF and a model bow shock. Integrating between two positions x_1 and x_2, we obtain

$$\ln\frac{\Gamma_E(x_2)}{\Gamma_E(x_1)} = -\sigma(E)\int_{x_1}^{x_2} n_H(r(x))dx \tag{2}$$

The features shown on Figure 1 are common upstream of the Mars bow shock, particularly when the magnetic field direction is nearly radial. Figure 3 shows another event observed on 29 January 2015 between 1630 UT

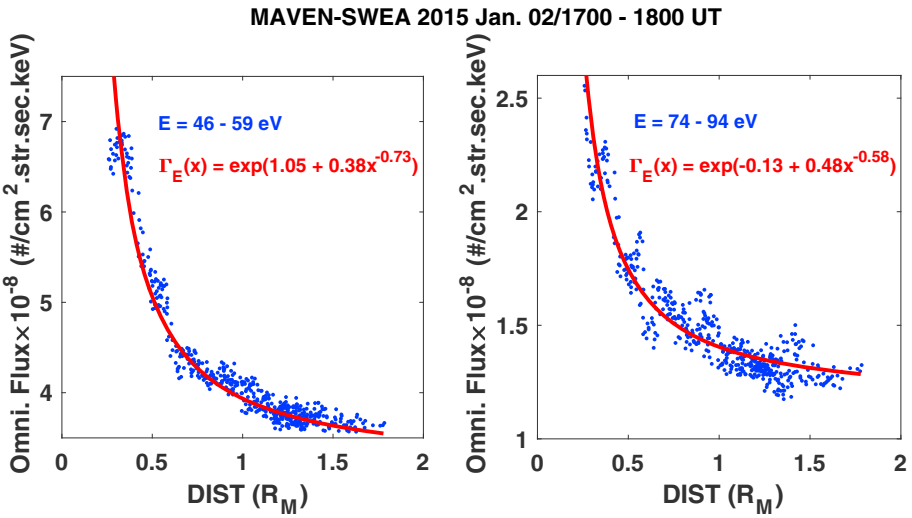

Figure 2. Scatter plot of electron flux versus *DIST* for two energy ranges. The continuous red curve represents the best fit with a function $y = \exp(a + bx^{-\beta})$.

and 1720 UT which depicts very similar features as Figure 1: SWEA electron flux decrease for an energy above $E \geq 30$ eV with distance upstream of the bow shock. Again, the model used here (Vignes et al., 2000) fits quite well the MAVEN bow shock crossing of Mars. Such good agreement has been obtained for the other cases analyzed up to now, and this justifies a posteriori the use of such a static statistical model.

The theoretical determination of the flux $\Gamma_E(x)$ requires an explicit profile $n_H(r(x))$ in terms of x. The first in situ measurements of density, composition, and temperature in the Mars exosphere were carried out by Mariner 5, 6, and 9 spacecraft and the Viking landers (Barth et al., 1971; Nier & McElroy, 1977). Later observations by various spacecraft including Mars Express, allowed a reliable determination of Mars exospheric hydrogen and oxygen density at various altitudes (Chaufray et al., 2008, 2009). These determinations were also supported by theoretical studies. In the case of exospheric hydrogen, the measurements are usually based on mapping of HI Lyman α and Lyman β emissions. During the Rosetta gravity assist swing-by of Mars, Feldman et al. (2011) used the Alice far-ultraviolet spectrometer to map H1 Lyman α and H1 Lyman β up to $\sim 9R_M$ from the planet center. Using a spherical Chamberlain model, the authors were able to derive a model for both the exospheric hydrogen and oxygen density profiles. For distances of interest within the Martian foreshock, the Feldman et al. (2011) exospheric hydrogen density profile scales as $\sim r^{-\alpha}$, with $\alpha \sim 2.1$. More recently, Chaffin et al. (2015) have presented unique observations from the Imaging Ultraviolet Spectrograph on MAVEN (McClintock et al., 2015) of the Mars H corona to large radial distances and mapping results from initial science at Mars. These observations represented the first detection of three-dimensional structure in the H corona of Mars showing it cannot be reproduced by a simple spherical model. However, this does not provide any analytical form for the hydrogen density profile, and as a first step, a simpler approach is used here. For field-aligned electron dynamics, the use of distance $x = DIST$ provides the appropriate geometry for the electron flux attenuation rather than the planetocentric distance r used in a density profile model. In general, the change of x results from IMF variations as well as the orbital motion of the spacecraft, and it is straightforward to show $r \approx c_1 + c_2 x$, where c_1 and c_2 vary with the direction of the IMF and the spacecraft position. Therefore, using the hydrogen density profile $n_H(r(x))$ to determine the electron flux decrease from equation (2) remains problematic. On the other hand, and for instructive reasons, an attempt to determine an analytical approximation form for the electron variation versus distance may be pertinent. One way is to fit the data shown on Figure 2, and it is reasonable to use by analogy a functional form for the electron flux as $\ln\Gamma_E(x) = a + bx^{-\beta}$, where a, b, and β are constant to be determined by the fit.

For the two energy ranges $E = 46$–59 eV and $E = 74$–94 eV, the result of the fit is shown with the red curve on Figure 2 on which the constants of the fit are reported. The fit is quite reasonable and it provides χ^2 values of 0.68 and 1.37, respectively. Using the same functional form for the flux with a constant exponent $\beta = 1.1$, a similar satisfactorily fit to the data is obtained with very close χ^2 numerical values, respectively, 0.89 and 1.58. It results that using $\beta \approx \alpha - 1$ as obtained from the approximation $n(r) \approx n(x)$ could be adequately used

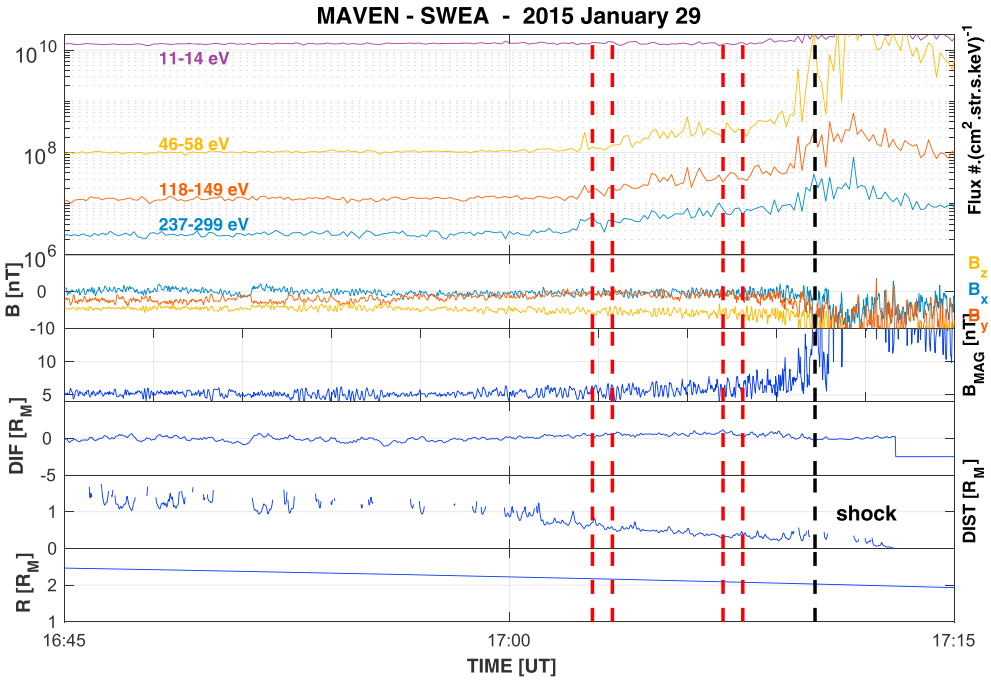

Figure 3. Same format as Figure 1 for 29 January 2015/1645–1715 UT time interval.

to integrate expression 2. Clearly, the decline of the electron flux versus distance from the shock is not linear and may reflect the electron impact with the exospheric hydrogen which density profile is consistent with Feldman et al.'s (2011) model.

Pursuing the analysis further and in order to better adjust a comparison of equation (1) with the observations, the dependence upon the bow shock and hydrogen profile models is eliminated. For this purpose, expression (2) is formulated for two arbitrary energy values E_1 and E_2 and the following ratio is derived:

$$\xi = \frac{\ln \frac{\Gamma_{E_1}(x_1)}{\Gamma_{E_1}(x_2)}}{\ln \frac{\Gamma_{E_2}(x_1)}{\Gamma_{E_2}(x_2)}} = \frac{\sigma(E_1)}{\sigma(E_2)} \tag{3}$$

Hence, the ratio ξ is solely dependent upon the electron flux levels and therefore can be directly obtained from observations. The right-hand term of equation (3) can also be determined from ionization cross-section tables. Taking $E_1 = E$ and an arbitrary fixed reference energy $E_2 = E_0$, we derive the energy-dependent ratio:

$$\xi_{E_0}(E) = \frac{\sigma(E)}{\sigma(E_0)} \tag{4}$$

To plot the ratio $\xi_{E_0}(E)$ versus energy E, the electron flux level at each energy is selected at two instants t_1 and t_2 corresponding to distances x_1 and x_2, respectively, from the shock. In order to suppress noise in the flux measurements, we consider the flux level averaged over $\delta t \sim 20$ s (about 10 snapshots) centered on t_1 and t_2. These time intervals are indicated on Figure 1 by the two dual vertical red dashed lines.

Figure 4 shows the $\xi_{E_0}(E)$ ratio as obtained from observations versus energy for $E_0 = 52.1$ eV, a numerical value corresponding to the maximum electron-hydrogen impact cross section. However, the results are only weakly sensitive to the choice of E_0.

Electron impact ionization cross sections of atoms are widely used for various reasons. Quantum mechanics provides the theoretical framework to describe the interaction of electrons with atoms. The case of electron impact with hydrogen has received a complete theoretical treatment (Baertschy et al., 2001), but the cases involving higher atomic number atoms and molecules are approached with approximations. Experimental measurements of electron impact cross sections provide sufficient precision for many applications, including the case here. Several laboratory measurements of the electron-neutral hydrogen impact can be found

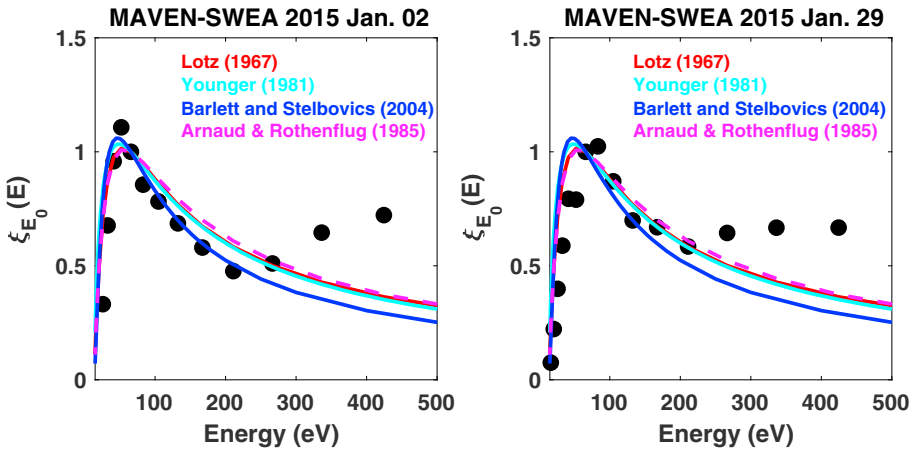

Figure 4. Black circles indicate $\xi_{E_0}(E)$ ratio versus E with $E_0 = 52.1$ eV. The continuous lines show the ratio of HI-electron impact cross sections $\frac{\sigma(E)}{\sigma(E_0)}$ from various sources.

in the literature (Arnaud & Rothenflug, 1985; Barlett & Stelbovics, 2004; Dixon et al., 1975; Lotz, 1967; Younger, 1981). Some of these provide convenient analytic functions that fit the data well. A good agreement exists between various laboratory determinations. Using tables available in the literature, the $\frac{\sigma(E_1)}{\sigma(E_2)}$ ratio versus energy E is superposed with data of Figure 4. As predicted by equation (3), the empirical cross section tracks well the observed flux ratio for electron energy $E \leq 250$ eV. At higher electron energy, a significant departure from the cross-sections ratio curve exists.

The above results may have important implications for the pickup ion production rate at Mars, which can be significant beyond the bow shock. In particular, the foreshock may contribute to exospheric loss resulting from the pickup process, as explained in section 1. Particularly, the relative contribution of the foreshock electron impact ionization process could be compared with the photoionization and charge exchange mechanisms. Such detailed investigation is beyond the present study. Interestingly, the ULF wave amplitude related to the pickup protons (near to the proton cyclotron frequency (Romanelli et al., 2015)) display clear variations for each electron foreshock crossing (an example is given on Figure 3 of Meziane et al. (2017)). Since the source of the waves come from the pickup protons, this observed feature could reflect the process demonstrated by the present study which should be relatively important. When MAVEN crosses the bow shock, it can spend an important part of its upstream orbit inside the foreshock depending on the geometry, the largest relative duration being observed for quasi-radial IMF. This will be the topic of a future study.

5. Conclusion

The decrease of foreshock electron flux with distance from the shock is an important feature of Mars's foreshock. The mechanisms related to the reflection at the shock and the scattering by plasma waves and magnetic field fluctuations do not account for the observed flux gradual decrease. Using a simple attenuation model, quantitative arguments are provided to support the interpretation that the flux decline results from electron impact with exospheric atomic hydrogen upstream of the bow shock. While the model provides satisfactory results for energies where the scattering cross section is maximum, it remains poor at high energy. At first glance, the effect due to electron impact with oxygen does not seem to account for the departure seen at high energy. The exospheric oxygen density remains relatively small and the maximum impact cross section occurs at an energy significantly less than 250 eV. It however requires in-depth prospects before making any conclusion. This point will be addressed in a future work. This result may have important implications on the pickup ion production rate at distance far from the planet center. Also, additional pickup ion production rate due to the electron impact inside the electron foreshock is an important element in our comprehensive understanding of the Martian upstream region variability at small time scales compared to seasonal effects on much larger time scales reported on pickup ions by Yamauchi et al. (2015) and associated ULF waves by Romanelli et al. (2015). Moreover, the experimental flux attenuation-fitted profiles could be used as a new tool to constrain the exospheric hydrogen density profiles [by the inversion of equation (2)], and this will be also investigated in a future study. Eventually, the reported observations have been obtained in the most

favorable season for the H exosphere when the densities are the highest (Clarke et al., 2017; Halekas et al., 2017; Rahmati et al., 2017; Romanelli et al., 2015). It will be necessary to check whether the same effect is observable during the low season where the hydrogen density is reduced by one order of magnitude.

Acknowledgments
MAVEN data are publicly available through the Planetary Data System. This work is supported by the French space agency CNES for the observations obtained with the SWEA instrument. K. M. wishes to express his thanks to the IRAP in Toulouse for the support in the collaboration work on MAVEN. Work at UNB is supported by the Canadian Natural Science and Engineering Council.

References

Arnaud, M., & Rothenflug, R. (1985). An updated evaluation of recombination and ionization rates. *Astronomy and Astrophysics Supplement Series*, *60*, 425–457.

Baertschy, M., Resigno, T. N., Issacs, W. A., Li, X., & McCurdy, C. W. (2001). Electron-impact ionization of atomic hydrogen. *Physical Review A*, *63*, 022712.

Brain, D. A., & Jakosky, B. M. (1998). Atmospheric loss since the onset of the Martian geologic records: Combined role of impact and sputtering. *Journal of Geophysical Research*, *103*, 22,689–22,694. https://doi.org/10.1029/98JE02074

Barlett, P. L., & Stelbovics, A. T. (2004). Electron-impact ionization cross sections for elements $Z = 1$ to $Z = 54$. *Atomic Data and Nuclear Data Tables*, *86*, 235–265.

Barth, C. A., Hord, C. W., Pearce, J. B., Kelly, K. K., Anderson, G. P., & Stewart, A. I. (1971). Mariner 6 and 7 ultraviolet spectrometer experiment: Upper atmosphere data. *Journal of Geophysical Research*, *76*, 2213–2227.

Chaffin, M. S., Chaufray, J. Y., Deighan, J., Schneider, N. M., McClintock, W. E., Stewart, A. I. F., et al. (2015). Three-dimensional structure in the Mars H corona revealed by IUVS on MAVEN. *Geophysical Research Letters*, *42*, 9001–9008. https://doi.org/10.1002/2015GL065287

Chaufray, J. Y., Bertaux, J. L., Leblanc, F., & Quémerais, E. (2008). Observation of the hydrogen corona with SPICAM on Mars Express. *Icarus*, *195*, 598–613.

Chaufray, J. Y., Leblanc, F., Quémerais, E., & Bertaux, J. L. (2009). Martian oxygen density at the exobase deduced from O I 130.4-nm observations by spectroscopy for the investigation of the characteristics of the atmosphere of Mars on Mars Express. *Journal of Geophysical Research*, *114*, E02006. https://doi.org/10.1029/2008JE003130

Chen, F. F. (1984). *Introduction to plasma physics and controlled fusion* (Vol. 1). New York: Plenum Press.

Clarke, J. T., Mayyasi, M., Bhattacharyya, D., Schneider, N. M., McClintock, W. E., Deighan, J. I., et al. (2017). Variability of D and H in the Martian upper atmosphere observed with the MAVEN IUVS echelle channel. *Journal of Geophysical Research: Space Physics*, *122*, 2336–2344. https://doi.org/10.1002/2016JA023479

Connerney, J. E. P., Espley, J., Lawton, P., Murphy, S., Odom, J., Oliversen, R., & Sheppard, D. (2015). The MAVEN magnetic field investigation. *Space Science Reviews*, *195*, 257–291. https://doi.org/10.1007/s11214-015-0169-4

Dixon, A. J., Von Engel, A., & Harrison, M. F. A. (1975). A measurement of the electron impact ionization cross section of atomic hydrogen in the metastable 2S state. *Proceedings of the Royal Society of London. Series A, Mathematical and Physical Sciences*, *343*(1634), 333–349.

Feldman, P. D., Steffl, A. J., Parker, J. W., A'Hearn, M. F., Bertaux, J.-L., Alan Stern, S., et al. (2011). Rosetta-Alice observations of exospheric hydrogen and oxygen on Mars. *Icarus*, *214*, 394–399. https://doi.org/10.1016/j.icarus.2011.06.013

Halekas, J. S., Ruhunusiri, S., Harada, Y., Collinson, G., Mitchell, D. L., Mazelle, C., et al. (2017). Structure, dynamics, and seasonal variability of the Mars-solar wind interaction: MAVEN Solar Wind Ion Analyzer in-flight performance and science results. *Journal of Geophysical Research: Space Physics*, *122*, 547–578. https://doi.org/10.1002/2016JA023167

Jakosky, B. M., Lin, R. P., Grebowsky, J. M., Luhmann, J. G., Mitchell, D. F., Beutelschies, G., et al. (2015). The MAVEN mission to Mars. *Space Science Reviews*, *195*, 3–48. https://doi.org/10.1007/s11214-015-0139-x

Leroy, M. M., & Mangeney, A. (1984). A theory of energization of solar wind electrons by the Earth's bow shock. *Annals of Geophysics*, *2*, 449–456.

Lotz, W. (1967). Electron-impact ionization cross-sections and ionization rate coefficients for atoms and ions. *The Astrophysical Journal Supplement Series*, *14*, 207–238.

Lundin, R., Zakharov, A., Pellinen, R., Borg, H., Hultqvist, B., Pissarenko, N., et al. (1989). First measurements of the ionospheric plasma escape from Mars. *Nature*, *341*(6243), 609–612. https://doi.org/10.1038/341609a0

McClintock, W. E., Schneider, N. M., Holsclaw, G. M., Clarke, J. T., Hoskins, A. C., Stewart, I., et al. (2015). The imaging ultraviolet spectrograph (IUVS) for the MAVEN mission. *Space Science Reviews*, *195*, 75–124. https://doi.org/10.1007/s11214-014-0098-7

Meziane, K., Mazelle, C. X., Romanelli, N., Mitchell, D. L., Espley, J. R., Connerney, J. E. P., et al. (2017). Martian electron foreshock from MAVEN observations. *Journal of Geophysical Research: Space Physics*, *122*, 1531–1541. https://doi.org/10.1002/2016JA023282

Mitchell, D. L., Mazelle, C., Sauvaud, J.-A., Thocaven, J.-J., Rouzaud, J., Fedorov, A., et al. (2016). The MAVEN solar wind electron analyzer. *Space Science Reviews*, *200*, 495–528. https://doi.org/10.1007/s11214-015-0232-1

Nier, A. O., & McElroy, M. B. (1977). Composition and structure of Mars' upper atmosphere: Results from the neutral mass spectrometers on Viking 1 & 2. *Journal of Geophysical Research*, *82*, 4341–4149. https://doi.org/10.1029/JS08i028p04341

Rahmati, A. (2016). Oxygen exosphere of Mars: Evidence from pickup ions measured by MAVEN (PhD dissertation). Department of Physics and Astronomy, University of Kansas.

Rahmati, A., Larson, D. E., Cravens, T. E., Lillis, R. J., Halekas, J. S., McFadden, J. P., et al. (2017). MAVEN measured oxygen and hydrogen pick up ions: Probing the Martian exosphere and neutral escape. *Journal of Geophysical Research: Space Physics*, *122*, 3689–3706. https://doi.org/10.1002/2016JA023371

Romanelli, N., Mazelle, C., Chauffray, J. Y., Meziane, K., Shan, L., Ruhunusiri, S., et al. (2015). Proton cyclotron waves occurrence rate upstream from Mars observed by MAVEN: Associated variability of the Martian upper atmosphere. *Journal of Geophysical Research: Space Physics*, *121*, 11,113–11,128. https://doi.org/10.1002/2016JA023270

Vandas, M. (2001). Shock drift acceleration of electrons: A parametric study. *Journal of Geophysical Research*, *106*, 1859–1871. https://doi.org/10.1029/2000JA900128

Vignes, D., Mazelle, C. X., Rème, H., Acuña, M. H., Connerney, J. E. P., Lin, R. P., et al. (2000). The solar wind interaction with Mars: Locations and shapes of the bow shock and the magnetic pile-up boundary from the observations of the MAG/ER experiment onboard Mars Global Surveyor. *Geophysical Research Letters*, *27*(1), 49–52.

Yamauchi, M., Hara, T., Lundin, R., Dubinin, E., Fedorov, A., Sauvaud, J.-A., et al. (2015). Seasonal variation of Martian pick-up ions: Evidence of breathing exosphere. *Planetary and Space Science*, *119*, 54–61. https://doi.org/10.1016/j.pss.2015.09.013

Younger, S. M. (1981). Electron impact ionization cross sections and rates for highly ionized atoms. *Journal of Quantitative Spectroscopy & Radiative Transfer*, *26*, 329–337.